Article:
Wang, H, Jones, D, de Boer, G orcid.org/0000-0002-5647-1771 et al. (4 more authors) (2018) Design and Characterization of Tri-axis Soft Inductive Tactile Sensors. IEEE Sensors Journal, 18 (19). pp. 7793-7801. ISSN 1530-437X

https://doi.org/10.1109/JSEN.2018.2845131

This article has been accepted for publication in a future issue of this journal, but has not been fully edited. Content may change prior to final publication. Citation information: DOI 10.1109/JSEN.2018.2845131, IEEE Sensors Journal

Design and Characterization of Tri-axis Soft Inductive Tactile Sensors

Hongbo Wang, *member, IEEE*, Dominic Jones, Gregory de Boer, Junwai Kow, *student member*, *IEEE*
Lucia Beccai, *Member, IEEE*, Ali Alazmani, *member*, *IEEE*, and Peter Culmer, *Member, IEEE*

***Abstract*— Tactile sensors are essential for robotic systems to safely and effectively interact with the environment and humans. In particular, tri-axis tactile sensors are crucial for dexterous robotic manipulations by providing shear force, slip or contact angle information. The Soft Inductive Tactile Sensor (SITS) is a new type of tactile sensor that measures inductance variations caused by eddy-current effect. In this paper, we present a soft tri-axis tactile sensor using the configuration of four planar coils and a single conductive film with hyperelastic material in between them. The working principle is explained and design methods are outlined. A 3D finite element model was developed to characterize the tri-axis SITS and to optimize the target design through parameter study. Prototypes were fabricated, characterized and calibrated, and a force measurement resolution of 0.3 mN is achieved in each axis. Demonstrations show that the sensor can clearly measure light touch (a few mN normal force) and shear force pulses (10 to 30 mN) produced by a serrated leaf when it is moved across the sensor surface. The presented sensor is low cost, high performance, robust, durable, and easily customizable for a variety of robotic and healthcare applications.**

***Index Terms*—Eddy-current effect, Finite element analysis, Hyperelastic material, Inductance, Planar coil, Soft tactile sensor.**

I. Introduction

Tactile sensors are essential for robotic systems to interact safely, and effectively with the environment and humans [1, 2], and also they play a key role in intelligent healthcare systems [3-5]. Over the last decades, remarkable progress has been made in developing soft/flexible electronic skins [6, 7] for pressure mapping by exploiting a variety of transducer mechanisms (e.g.: piezoresistive [8], capacitive [9], and piezoelectric [10], triboelectric [11], and optical waveguide sensors [12]), and advances in organic electronics [13] and printed flexible electronics [14]. Nevertheless, tactile skins remain relatively un-developed for widespread use in robotics applications [15]. To be integrated into robots performing real-world applications, tactile sensors need to have both high compliance and high performance (like the human fingertip) and to be durable to survive the repeated physical interactions with unstructured environments [1]. Moreover, tactile sensors with tri-axis force sensing capabilities (mimicking human sense of touch) would significantly enhance the performance of robotic manipulations by providing shear and slip information [16, 17].

Recently, research to develop tri-axis tactile sensors and sensing arrays with 3D deformable structures has grown rapidly. Several notable examples can be acknowledged to provide an indication of state of the art. In 2012, a tri-axis resistive tactile sensor was developed by using embedded micro-channels filled with liquid metals [18]. This type of sensor is extremely stretchable, but it is complex to fabricate and only operates at temperatures above the melting point of the liquid metal. In 2014, a novel tri-axis capacitive tactile sensors with soft textile electrodes was developed [19], which has extremely high sensitivity and large dynamic range. While capacitive sensors usually encounter noise from proximity effect and environmental contaminants [20], a more complex shielding configuration is required to solve this issue. An alternative approach has exploited recent advances in integrated, compact, magnetic field sensing chips, the authors developed a tri-axis tactile sensor (MagOne [21, 22]) and sensing array (MagTrix [23]) using 3D Hall-effect sensors and magnets embedded in elastomer. Such sensors are soft, low-cost and capable of high-performance force sensing (resolution, dynamic range and bandwidth). However, they are inherently sensitive to static magnetic field interference from the environment or external ferromagnetic objects. Therefore, we sought to investigate alternative transducer mechanisms which could measure tri-axis force with high performance, robustness, and simple structure.

Eddy-current sensors (ECS) are widely used for non-contact displacement measurement [24] and non-destructive testing systems [25] in harsh environments. In 2013, Wang et al. [26, 27] developed a sub-nanometer resolution eddy-current displacement sensor with self-compensation of thermal drift. By transforming the eddy-current effect-based sensing mechanism into a soft form for tactile sensing, we developed the first Soft Inductive Tactile Sensor (SITS) [28]. This initial work demonstrated that SITS has low hysteresis, good repeatability, wide bandwidth, and an ability to operate in harsh

An earlier version (3 pages) of this paper was presented at the IEEE Sensors 2017, Glasgow, UK, and was published in its proceedings (DOI: 10.1109/ICSENS.2017.8234098). This work was supported in part by the Leverhulme Trust (Grant number: RPG-2014-381), the EPSRC (Grant number: EP/R041776/1), and the Istituto Italianno di Tecnologia (IIT).

H. Wang and L. Beccai are with the Center for Micro-BioRobotics (CMBR@SSSA) of the Istituto Italiano di Tecnologia (IIT) in Pontedera (PI), 56025, Italy. (e-mail: Hongbo.Wang@iit.it, Lucia.Beccai@iit.it).

D. Jones, G. de Boer, J. Kow, A. Alazmani, and P. Culmer are with the school of mechanical engineering, the University of Leeds, Leeds, LS2 9JT, UK. (e-mail: mn11dpj@leeds.ac.uk, G.N.deBoer@leeds.ac.uk, el11jwk@leeds.ac.uk, A.Alazmani@leeds.ac.uk, P.R.Culmer@leeds.ac.uk).

This article has been accepted for publication in a future issue of this journal, but has not been fully edited. Content may change prior to final publication. Citation information: DOI 10.1109/JSEN.2018.2845131, IEEE Sensors Journal

environments (e.g. underwater). Furthermore, STIS has a simple structure, can be readily fabricated in a durable form (see the hammer strike test in supplementary materials) for real world applications. Building on this single-axis system, we developed the first tri-axis SITS using a configuration of four coils and a single target [29], which achieved a force measurement resolution of 0.3 mN in each axis.

In this paper, we extend the work presented in [29] to describe the system in detail, includes the sensor design, modelling, prototype characterization and calibration, demonstrations of the performance. The paper begins by describing the underpinning working principle of the sensors, then uses a finite element (FE) model to investigate key design parameters of the tri-axis SITS system, the optimized target design is obtained. Prototypes and the associated electronic interfaces are developed based on these design methods. Prototype systems were characterized and calibrated, cross-talk effect and non-linearity are minimized, the decoupled output shows good match against a commercial force/torque sensor. Demonstration tests are performed to highlight the tri-axis sensing capabilities and the high-performance in real-world applications.

II. Working Principle

A. Single-Axis SITS

Transducers based on the mechanism of Eddy-current effect are ubiquitous in industry, particularly in the form of non-contact eddy-current displacement sensors. As illustrated in Fig. 1(a), an ECS comprises a coil as sensing unit, and a conductive film as sensing target, which is typically used to measure the vertical distance between the sensing coil and the conductive target. When the coil is excited by an AC current (typically at 0.1 MHz to 10 MHz), it generates an alternating magnetic field which induces eddy-currents in the nearby conductive target. The eddy-currents in the target generate a magnetic field opposite to that from the coil, thus reducing the magnetic flux in the coil and dissipating energy. Therefore, this magnetic field coupling between the coil and the target reduces the coil's inductance and increases its resistance. Thus, the vertical distance (d_z) between the coil and the target can be obtained by measuring the inductance of the coil. Figure 1(b) shows the normalized inductance and resistance versus distance characteristics of a typical ECS.

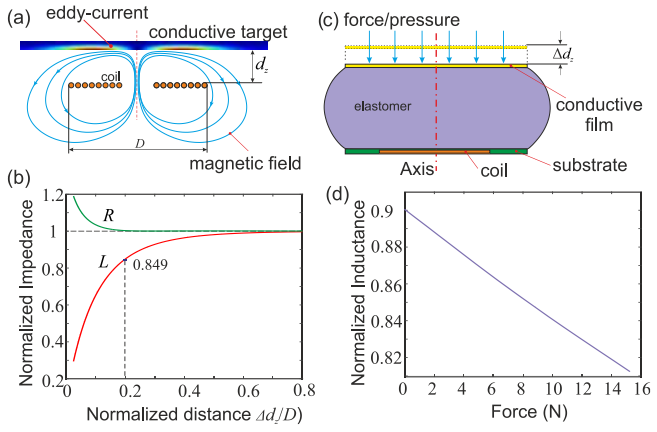

Fig. 1. (a) Working principle of a typical eddy-current sensor (ECS); (b) Normalized impedance to distance response of an ECS; (c) Schematic of single-axis soft inductive tactile sensor (SITS); (d) Normalized inductance to force response of a SITS.

A soft inductive tactile sensor (SITS) can be adapted from the ECS by introducing an elastic medium between the coil and the target, which acts to modulate the distance when force is applied to the target, as shown in Fig. 1(c). Figure 1(d) shows the inductance to force response of a single-axis SITS. The conductive target acts as both sensing target and an electromagnetic shielding layer, which minimizes the interference from external objects. As discussed in our previous paper [30], the conductive film should have a diameter greater than the excitation coil and a thickness larger than the eddy-current penetration depth [31] (26.5 μm for copper at 6 MHz) to achieve both good sensitivity and effective electromagnetic shielding.

B. Tri-Axis SITS

When the target does not completely cover the effective sensing area, lateral position of the coils can also affect the inductance, due to the variation of magnetic field coupling between the coil and target. As illustrated in Figure 2(a-c), for a rectangular, triangular, or small circular target, moving the target laterally changes the magnetic field coupling, thereby the inductance. Since the eddy-current intensity is also highly dependent on the vertical distance between the coil and the target, both lateral and vertical movements of the target can cause measurable inductance variation. A single coil SITS with targets illustrated in Fig. 2(a-c) is sensitive to both normal and shear forces, but it cannot discriminate them.

Here, we propose a four-coil array to detect the tri-axis movement of a square conductive target. As shown in Fig. 2(d), when the target is moved along *x*-axis, the target's magnetic field coupling with *coil 1* and *coil 4* increases, while the coupling with *coil 2* and *coil 3* decreases. The same principle applies in the *y*-axis. When the vertical distance decreases, the coupling with all four coils increases. As illustrated in Fig. 2(e), when an external force is applied, the conductive film is moved

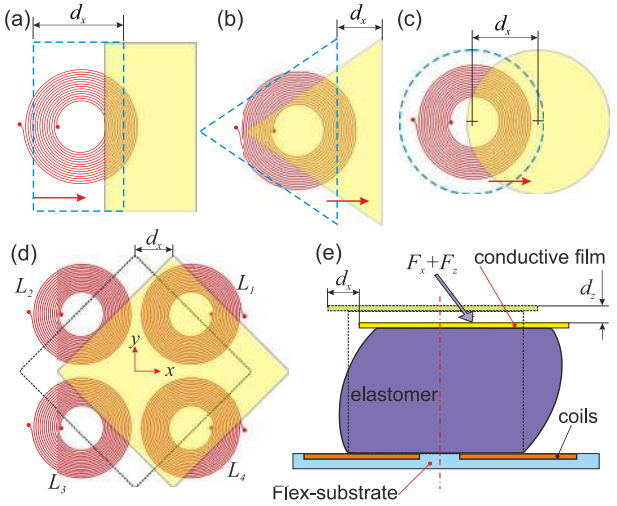

Fig. 2. ECS for vertical displacement measurement with different target shape (a) Rectangular; (b) Triangular; (c) Circle; (d) Tri-axis ECS configuration using four coils and one target; (d) Schematic of a tri-axis SITS.

This article has been accepted for publication in a future issue of this journal, but has not been fully edited. Content may change prior to final publication. Citation information: DOI 10.1109/JSEN.2018.2845131, IEEE Sensors Journal

vertically/laterally through deformation of the elastomer, which changes the inductance of all four coils. The relationship between L_1, L_2, L_3, and L_4 and the applied force F_x, F_y, and F_z is complex because of the highly nonlinear response of ECSs (Fig. 1(b)) and the strong cross-talk effect between axes. However, a decoupled output signal can be approximated by calculating the differential inductance between coils (similar to balancing resistance in a Wheatstone bridge [32]):

$$\begin{cases} L_x = L_1 - L_2 - L_3 + L_4 \\ L_y = L_1 + L_2 - L_3 - L_4 \\ L_z = L_1 + L_2 + L_3 + L_4 \end{cases} \quad (1)$$

III. Design and Modelling

As discussed in our previous papers [21], the design of tri-axis SITS can also be divided in two steps. The first is to design the inductive transducer to measure the tri-axis displacement of the conductive target. The second step is to choose the elastomer geometry and material to achieve desired sensitivity and force measurement range. The mechanical behavior of the elastomer body is known, and has been investigated in our previous papers on MagOne sensor [21, 22] and single-axis STIS sensor [28]. In this section, we will focus on the design of the tri-axis inductive displacement transducer, which forms the core of a tri-axis SITS.

A. Sensor Design

To characterize the sensor's response and investigate the design parameters of the tri-axis SITS, the sensing coil design was determined first. As shown in Fig. 3(a), each sensing coil has two layers, with 12 turns per layer and an outer diameter of 7.0 mm. Considering the capabilities of most flexible printed circuit (FPC) manufactures, the coil loop has a trace width of 100 µm, thickness of 35 µm, and a spiral pitch of 200 µm (100 µm space between two traces), same as the single-axis SITS [28]. Two layers of loops are in series connection in a way that all loops have the same current direction. The distance between coils is 8 mm to minimize the device size and also ensure that coils are not overlapped. A square target is configured in 45º with the coordinate axis so that it covers approximately half area of each coil (Fig. 3(b)). The lateral position of the target from the coil center is denoted as d_x, while the vertical distance is d_z.

B. FE Modelling and Results

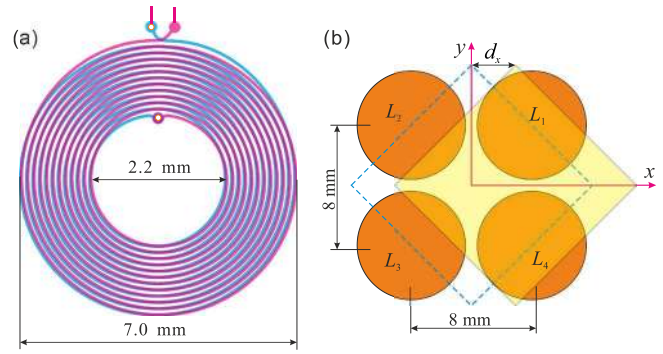

Fig. 3. (a) Schematic of the double layer spiral coil design; (b) Dimension and configuration of the target and coils of the tri-axis SITS.

To investigate the characteristics and key design parameters of this tri-axis SITS, a 3D FE model with the coil, target and air domains was built in COMSOL Multiphysics (AC/DC module). Frequency domain study of the 3D FE model was performed at 6 MHz (approximate the working frequency of the physical device) to calculate the effective inductance and AC resistance of the coil-target pair. As four coils were excited in sequence in the SITS prototypes, only one coil is carrying the AC current and has magnetic field coupling with the target at any one time. Given the symmetric coil-target configuration, *coil 4* has exact the same response to d_z/d_x as *coil 1*, while *coil 2*'s response to d_z/d_x can be calculated from *coil 1*'s response by

$$L_2(d_z, d_x) = L_1(d_z, -d_x) \quad (2)$$

The same principle can be applied to movement in the *y* axis as well. Therefore, to minimize the computational time, only *coil 1* was built and driven with a 1 mA AC current in the 3D FE model. The normalized inductance of *coil 1* to vertical and lateral movement of the target was calculated. As plotted in Fig. 4 (a), when the target to coil distance decreases from 3 mm to 1 mm, *coil 1*'s inductance variation is larger when the target covers larger area of the coil at 1 mm lateral position (d_x) than at -1 mm. Figure 4(b) shows that *coil 1*'s inductance decreases when the target-coil overlap area increases (target moves from -2 mm lateral position to 2 mm). While the inductance variation caused by lateral movement of the target is highly dependent on the vertical distance (d_z) as eddy-current intensity decreases rapidly with d_z. The inductance to d_z/d_x response of *coil 2*, *coil 3* and *coil 4* can be calculated from *coil 1*'s data using equation (2). Then, the tri-axis inductance (L_x, L_y, and L_z) were calculated by equation 1. As shown in Fig. 4(c), the *z*-axis inductance variation (ΔL_z) to vertical distance (d_z) curves at

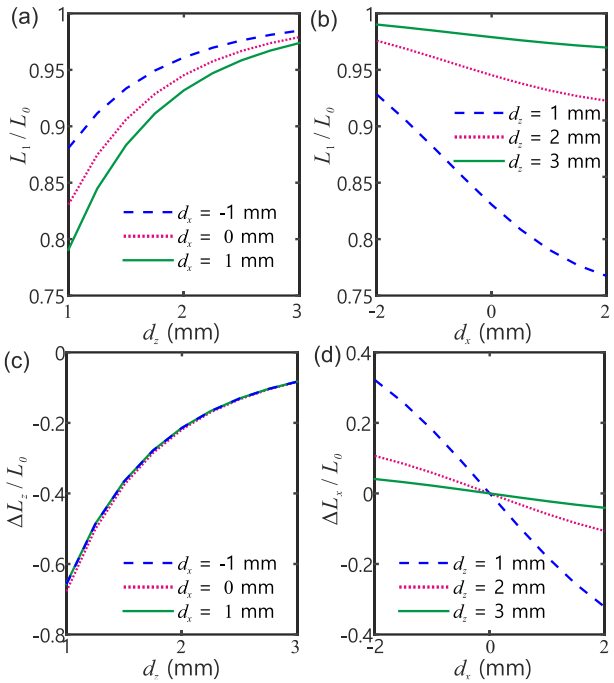

Fig. 4. Characterization of the tri-axis SITS using 3D FE model (a) Coil 1's inductance response to vertical distance of the target; (b) Coil 1's inductance response to lateral movement of the target; (c) Total inductance variation (ΔL_z) to vertical distance; (d) Total inductance (ΔL_x) to lateral movement of the target.

This article has been accepted for publication in a future issue of this journal, but has not been fully edited. Content may change prior to final publication. Citation information: DOI 10.1109/JSEN.2018.2845131, IEEE Sensors Journal

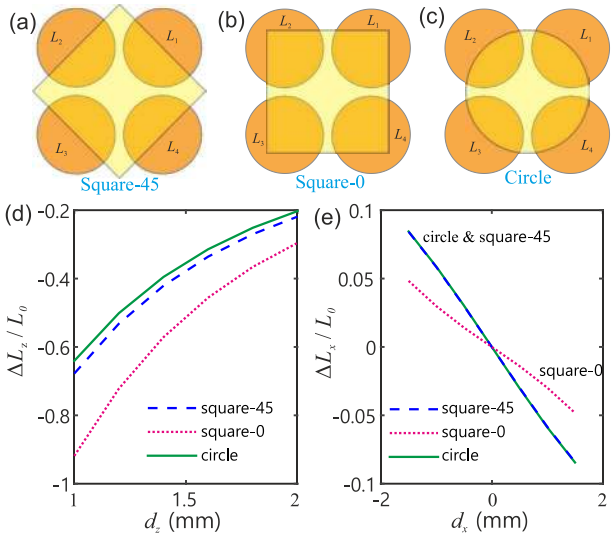

Fig. 5. Tri-axis SITS with different target shape configuration and response (a) square-shape target in 45 configuration; (b) square-shape target in 0 configuration; (d) Circle-shape target; (d) Total inductance variation (ΔL_z) to lateral distance response (d_x = 0 mm); (e) Total inductance variation (ΔL_x) to vertical movement (d_z = 2 mm).

different lateral position (d_x) are almost overlapped despite the different magnetic field couplings between the target and individual coil. The ΔL_x to d_x curves in Fig. 4(d) clearly show that the sensor with smaller vertical distance has better sensitivity to lateral displacement. As discussed in the single-axis SITS design [28], a thinner elastomer leads to a higher overall stiffness and limited deformation, which would result in a larger force range, but also a poorer sensitivity, despite its higher inductance to displacement sensitivity. The same principle is applicable for tri-axis SITS design. In this study, an elastomer thickness of 2 mm was selected to further investigate the conductive target design and prototyping.

C. Target Shape and Configuration

First, three representative target shape and configuration were investigated, including a square shape in 45º configuration, a square shape in 0º configuration, and a circular shape, named as "square-45", "square-0", and "circle" respectively. It is not necessary to design the target with a more complex shape (e.g. pentagon, hexagon or other irregular shapes) as it would be similar to one of these three cases, and irregular/asymmetric shape would just make the sensor's response more complex. Using the same FE model described above, the inductance to vertical distance (d_x) and lateral position (d_z) response was calculated for these three target design (side length of two squares and diameter of the circle are all 14 mm). Figure 5(d) shows that square-0 target has much higher sensitivity to vertical distance than square-45 and circle target because of its larger overlapped area between the coil and target compared to the other two. Square-45 and the circle target configurations have almost the same inductance variations to vertical distance. Moreover, the inductance response to lateral displacement of the square-45 and circle targets are completely overlapped, and their sensitivity are much higher than the square-0 configuration. Figure 5(d, e) also indicates that the inductance to displacement sensitivity in z-axis is higher than in x/y axis. Therefore, square-45 or circular

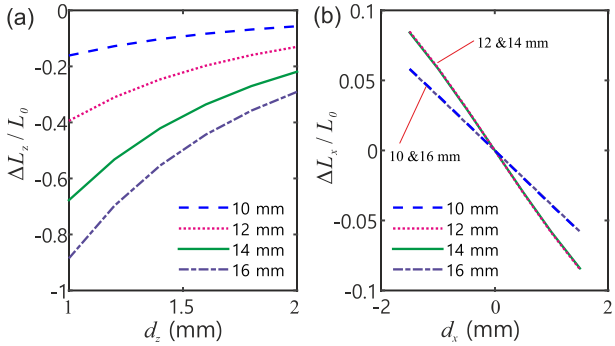

Fig. 6. Response of a tri-axis SITS with square-45 target in different size (a) Inductance variation (ΔL_z) to lateral distance response (d_x = 0 mm); (b) Inductance variation (ΔL_x) to vertical distance response (d_z = 2 mm).

target configuration should be used to develop tri-axis SITS with comparable sensitivity in all axes, particularly when a higher shear force sensitivity is desirable.

D. Target Size

To further study the size effect of the target, the square-45 target configuration with a side length from 10 mm, to 16 mm were investigated. Inductance variation to vertical distance d_z curves (Fig. 6(a)) clearly show that the larger the target size, the higher the sensitivity to z-axis movement since larger target size means stronger magnetic field coupling. As shown in Fig. 6(b), the response of 14 mm and 12 mm targets are completely overlapped, and have a higher sensitivity to d_x than 10 mm and 16 mm targets. When the target size is too small (e.g. 10 mm) the magnetic field coupling between the target and coils are too weak, while when the target size is too big (e.g. 16 mm), the magnetic field coupling is very strong, but the variation of the coupling strength is small when the target moves laterally. In summary, the sensitivity to lateral movement d_x increases with the target size first, then reach its maximum value at a target size between 12 mm to 14 mm, then decreases when the target size increases further. For this tri-axis SITS configuration, both 12 mm and 14 mm targets' design have higher shear force sensitivities, and the 14 mm target design has higher normal force sensitivity than the 12 mm one. Therefore, the 14 mm square target in 45º configuration would approximate the optimal design. Similar results are applicable for the circular target.

IV. PROTOTYPING

A. Fabrication

As described and analyzed in section III, a 2×2 coil array was designed for the tri-axis SITS. The flexible coils were fabricated by standard FPC process, have a total thickness of 0.2 mm. Figure 7(a) shows a magnified view of the fabricated flexible coil array. A 0.2 mm aluminum sheet was cut into 14 mm square and circle (ProtoLaser U3, LPKF laser and electronics AG, Germany) as sensing targets for tri-axis SITS prototypes. A uniform silicone sheet (2 mm thick, Ecoflex 00-20, Smooth-on, USA) was cast using a laser-cut plastic mold. Two parts of the silicone liquids were mixed by 1:1 weight and de-gassed, then poured into the mold to cure at room temperature. Then the cured silicone sheet was cut into 10

This article has been accepted for publication in a future issue of this journal, but has not been fully edited. Content may change prior to final publication. Citation information: DOI 10.1109/JSEN.2018.2845131, IEEE Sensors Journal

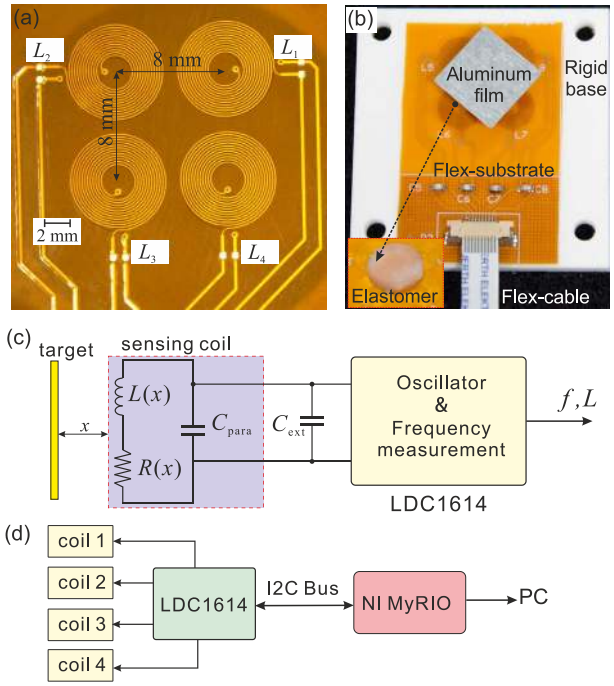

Fig. 7. (a) Magnified view of the flexible coils; (b) A tri-axis SITS prototype; (b) The inductance measurement circuit; (d) The electronic interface for the Tri-axis SITS prototype.

mm circle by a laser cutter (VLS 3.50, Universal laser systems). Finally, these elastomers were put into an ultrasonic isopropanol bath for 3 minutes to clean any ashes generated during the laser cutting. To assemble the tri-axis SITS prototype, the flexible coil sheet was glued to a rigid acrylic base with double side tape (3M, USA). Then, the aluminum target was glued to the elastomer with a thin layer of silicone adhesive (ELASTOSIL E 41, Wacker Chemie AG, Germany). Lastly, the elastomer-target structure was glued to the flexible coils with the same methods. Figure 7(b) shows an assembled SITS prototype with 14 mm square target in a 45º configuration.

B. Electronic Interface

In a complete tri-axis SITS system, the inductance of all four coils were measured at the working frequency. As shown in Fig. 7(c), the inductance measurement circuit of this sensor is based on a LC oscillator, the oscillating frequency of which varies with the coil's inductance:

$$f = \frac{1}{2\pi\sqrt{L\cdot(C_{para}+C_{ext})}} \quad (3)$$

where C_{para} is the parasitic capacitance of the coil (including cable), C_{ext} is an external capacitor used to form the oscillation network. A fully integrated, four channel, digital to inductance converter chip [33] (LDC1614, Texas Instruments, USA) was used to drive the oscillation network and measure its frequency, thereby the inductance. The coil-target pair has an inductance of approximately 3 μH (including cable) when it is unloaded. According to the guidelines summarized for the single-axis SITS [28], a 220 pF NP0 capacitor was used as the external capacitor to make the sensor work at a frequency of 6.2 MHz. Four coils are excited in sequence, the inductance measurement switches from one coil to another through a multiplexer integrated in LDC1614. The digital data were sent to a controller (NI MyRIO 1900, National Instruments, USA) via I²C protocol. The maximum sampling rate for this Tri-axis SITS can be up to 1 kHz by reducing the measurement time of inductance at the expense of increasing noise.

V. Experimental Results and Discussion

An experimental setup (the same platform used for the MagOne sensor [21]) was used to characterize and calibrate the tri-axis SITS. Which includes two motorized and one manual micro-positioning stages, and mounting frames/brackets to apply normal and/or shear force to the tri-axis SITS. A commercial force/torque sensor (Nano17-E, ATI industrial automation, USA) was mounted on the manual stage to record the applied normal and shear force as reference. A LabView program was developed to acquire and record data from the SITS prototypes and the Nano17 sensor, and to control the movement of two motorized stages.

A. Sensor Characterization

Firstly, the prototype was compressed by a rigid flat surface. Figure 8(a) shows the inductance variations of all four coils to applied normal force (0-13 N), which indicates that the inductance variations of these coils differ from one to another due to imperfect alignment of the target. To apply shear force to the tri-axis SITS prototype, a preload normal force of 8.4 N is applied. As shown in Fig. 8(b), *coil* 1 and *coil* 4's inductance decreases with the shear force in *x*-axis, while *coil 2* and *coil* 3's inductance increases. The decoupled inductance output to normal and shear force was calculated using equation (1) and plotted in Fig. 8(c, d), which shows that L_z (L_x) decreases rapidly with F_z (F_x), while there are small cross-talk effect between normal force and shear force output due to the

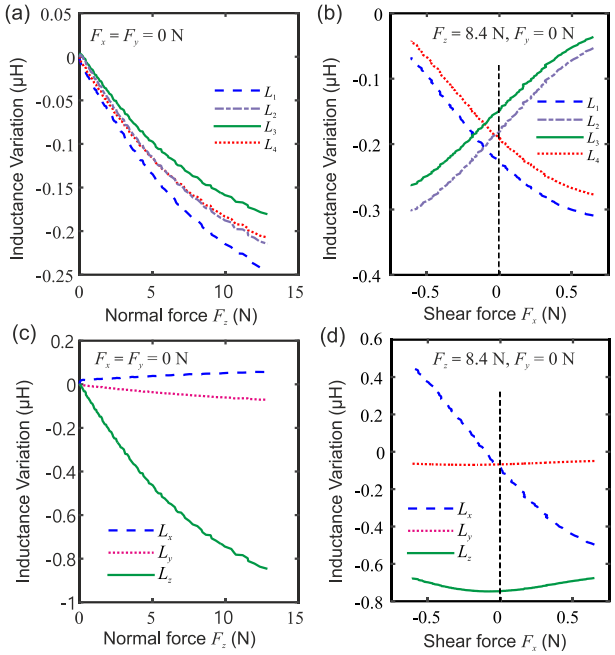

Fig. 8. Inductance variations of all four coils to the applied force (a) Normal force (0-13 N) (b) Shear force (0-1.4 N with 8.4 N preloaded normal force); Total inductance response to applied force (c) Normal force (0-13 N); (d) Shear force (0-1.4 N with 8.4 N preloaded normal force).

This article has been accepted for publication in a future issue of this journal, but has not been fully edited. Content may change prior to final publication. Citation information: DOI 10.1109/JSEN.2018.2845131, IEEE Sensors Journal

imperfect target configuration and elastomer shape. As shown in Fig. 8(c), the inductance L_x and L_y varies when normal force applied, but the variation is at least one order of amplitude less than ΔL_z.

B. Sensor Calibration

Given that the tri-axis SITS design is not axisymmetric, a 3D scanning process is required to fully investigate the relationship between the inductance and the applied force. The inductance response to lateral displacement in different directions was investigated using the 3D FE model (reported in section III) to quantify the response asymmetry to shear force. The FE results show that inductance response to lateral displacement at 45º to the x axis has a 4.89% lower sensitivity than in x/y axis (0º/90º direction) for a 14 mm square-45 target design (4.80% for a 14 mm circular target design). This state represents the maximum variability, and therefore, the tri-axis SITS design can be represented in simplified form as a sensor with an axisymmetric response and a two-parameter polynomial equation can be used to effectively describe the correlation between applied force and the output inductance:

$$\begin{cases} F_n = \sum_{k=0}^{n}\sum_{i=0}^{k} C_{zj} \cdot L_n^i \cdot L_s^{k-i} \\ F_s = \sum_{k=0}^{n}\sum_{i=0}^{k} C_{rj} \cdot L_n^i \cdot L_s^{k-i} \end{cases} \quad (4)$$

where F_n and F_s are normal and shear force respectively; C_{ik} are coefficients of the equation; n is the order of the polynomial; L_n (equals L_z) and L_s (equals $\sqrt{L_x^2 + L_y^2}$) are denoted to total normal and shear inductance. To obtain the calibration equation, a 2D scanning process (inset in Fig. 9(a)) was performed to collect a dataset of applied force and the corresponding inductance in *z-x* plane. Then, the least square error fitting technique described in [21] was employed to calculate these coefficients in equation (4) at n = 3. Thus, real-time calibrated force output can be obtained from the measured inductance values through equation (4) and (5).

$$\begin{cases} F_x = F_s \cdot L_x / \sqrt{L_x^2 + L_y^2} \\ F_y = F_s \cdot L_y / \sqrt{L_x^2 + L_y^2} \\ F_z = F_n \end{cases} \quad (5)$$

Figure 9(a, b) shows the calibrated normal force (F_z) and shear force (F_x) output respectively when the sensor's top surface is moved lateral to apply shear force while the normal force is increased incrementally (a preload normal force of approximately 7.3 N was applied to prevent slip). The results indicate a good match between the calibrated tri-axis SITS and the commercial sensor (Nano17). Noise testing results showed that the sensor has a resolution (minimum detectable force) of approximately 0.3 mN (50 Hz sampling rate) in all axes.

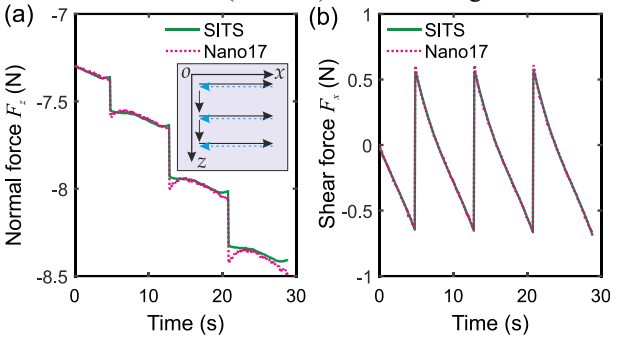

Fig. 9. Calibrated force output of the prototype compare with the reference force from Nano17 (a) Normal force, scanning path (inset).

C. Demonstration

To demonstrate the sensor's capability, a sensor prototype with a 12 mm square target in 45° configuration was fabricated and calibrated. A 2 mm bead was attached to the top surface of the sensor target to ensure single-point contact with a 3D printed surface. The surface consist of a planar base together with four sine profiles with 0.5 mm amplitude and 10 mm wavelength. The sensor was vertically positioned (upside down) and moved laterally across the sinewave surface at a rate of 1 mm/s. Calibrated normal/shear force was recorded and plotted in Figure 10(a), together with the surface height. It should be noted that the successive increase in force magnitude is the result of a slight slope in the surface.

To further demonstrate the sensor's high sensitivity in normal/shear force measurement, a new prototype with a 14 mm circular target was fabricated and calibrated. A leaf with serrated edge was moved across the sensor's top surface, and the calibrated tri-axis force output was recorded and plotted in Fig. 10. Shear force pulses (10 to 30 mN) caused by the serrated edges of the leaf were clearly measured. A normal force as small as a few mN was also observed due to the light touch of the leaf. This demo highlights the sensitivity and robustness of this tri-axis SITS for challenging tasks in real-world scenarios.

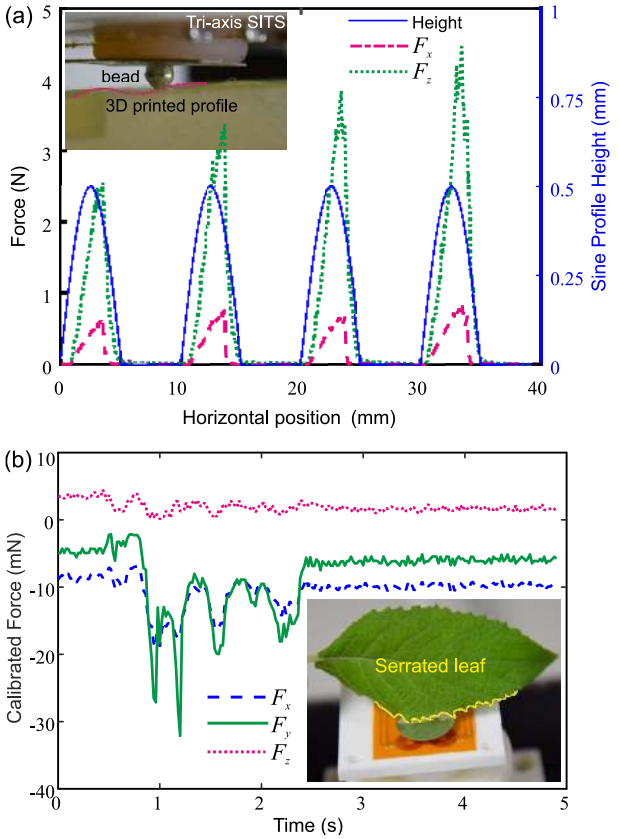

Fig. 10. Demonstrations: (a) The calibrated output of a tri-axis SITS with 12 mm square-45 target configuration moving against a sinusoidal profile; an image of the sensor and profile is shown (inset); (b) The output of a tri-axis SITS with 14 mm circular target when a serrated leaf was moved across the sensor surface; an image of the serrated leaf and the sensor prototype used for demonstration (inset).

This article has been accepted for publication in a future issue of this journal, but has not been fully edited. Content may change prior to final publication. Citation information: DOI 10.1109/JSEN.2018.2845131, IEEE Sensors Journal

D. Discussion

The design of the current SITS provides the ability to obtain sensitive tri-axis force measurements. For real world use, it is critical to characterize the sensor characteristics, calibrating against reference standards (to maintain consistent output across the measurement space and between sensors) and ensure sensor operation is not adversely affected by the environment.

A key aspect here is that the tri-axis SITS design is not axisymmetric, as stated in section V(B). When accurate shear force amplitude is required, a correction factor should be applied to equation (5) to minimize the error. Alternatively, a 3D scanning process could be performed to calibrate the sensor, which could require high computational cost. We have previously demonstrated that a Genetic Programming method [22] can be employed to optimally interpret the correlation between the measurand and sensor output value, establishing underlying trends and deriving robust and simple equations using training data. Subsequently, the coefficients of these equations for any sensor sharing the same design can be obtained efficiently through least squares regression.

It should be noted, in the current design, the sensor's output may be affected during interaction with conductive objects because the conductive target does not completely shield the full sensing area of all four coils. In this case, a conductive film or textile could be added as an upper shielding layer to address this issue. In addition, the current four coil design has one redundant degree of freedom which could be exploited for temperature drift compensation or noise suppression.

VI. CONCLUSION

In this paper, we presented a novel tri-axis tactile sensor based on inductance measurement which is low-cost, robust, easy to fabricate and capable of high sensitive measurement (0.3 mN resolution) for both normal and shear force. The working principle of the tri-axis SITS was described and the design principle was detailed. A 3D FE model was built to investigate the sensor's characteristics and optimize the target design through a parameter study. Sensing prototypes with electronics were developed and characterized in which a least-square error fitting technique was deployed to calculate coefficients of a polynomial equation that describes the correlation between the measured inductance value and the applied force. The calibrated prototypes demonstrate a good match for both normal and shear force measurement with the reference commercial sensor, but in soft form at far lower cost. Two demonstrations illustrate the high-performance and robustness of the tri-axis SITS for real-world applications.

The current SITS design can be scaled in size for a variety of robotic and healthcare applications. On the other hand, soft inductive sensors with sensing capabilities in more axes can be developed for deformable and robust force/torque sensors. For instance, a low-cost, six-axis force/torque sensors with high performance and high tolerance to overloading would be highly demanded. Finally, new materials and fabrication techniques offer opportunities to produce "fully soft" tri-axis tactile sensors and improve the durability of this system to enable robust physical interactions from the delicate (e.g. surgical robots) to harsh (field, industry, or rescue robots) scenarios.

REFERENCES

[1] C. Bartolozzi, L. Natale, F. Nori *et al.*, "Robots with a sense of touch," *Nature Materials,* vol. 15, no. 9, pp. 921-925, 2016.

[2] R. S. Dahiya, G. Metta, M. Valle *et al.*, "Tactile sensing—from humans to humanoids," *Robotics, IEEE Transactions on,* vol. 26, no. 1, pp. 1-20, 2010.

[3] P. Saccomandi, E. Schena, C. M. Oddo *et al.*, "Microfabricated tactile sensors for biomedical applications: a review," *Biosensors,* vol. 4, no. 4, pp. 422-448, 2014.

[4] J. Konstantinova, A. Jiang, K. Althoefer *et al.*, "Implementation of tactile sensing for palpation in robot-assisted minimally invasive surgery: A review," *IEEE Sensors Journal,* vol. 14, no. 8, pp. 2490-2501, 2014.

[5] L. Y. Chen, B. C.-K. Tee, A. L. Chortos *et al.*, "Continuous wireless pressure monitoring and mapping with ultra-small passive sensors for health monitoring and critical care," *Nature communications,* vol. 5, 2014.

[6] A. Chortos, J. Liu, and Z. Bao, "Pursuing prosthetic electronic skin," *Nature Materials,* vol. 15, no. 9, pp. 937-950, 2016.

[7] X. Wang, L. Dong, H. Zhang *et al.*, "Recent progress in electronic skin," *Advanced Science,* vol. 2, no. 10, 2015.

[8] L. Pan, A. Chortos, G. Yu *et al.*, "An ultra-sensitive resistive pressure sensor based on hollow-sphere microstructure induced elasticity in conducting polymer film," *Nature communications,* vol. 5, 2014.

[9] H.-K. Lee, J. Chung, S.-I. Chang *et al.*, "Real-time measurement of the three-axis contact force distribution using a flexible capacitive polymer tactile sensor," *Journal of Micromechanics and Microengineering,* vol. 21, no. 3, pp. 035010, 2011.

[10] J. H. Lee, H. J. Yoon, T. Y. Kim *et al.*, "Micropatterned P (VDF‐TrFE) Film‐Based Piezoelectric Nanogenerators for Highly Sensitive Self‐Powered Pressure Sensors," *Advanced Functional Materials,* vol. 25, no. 21, pp. 3203-3209, 2015.

[11] X. Wang, H. Zhang, L. Dong *et al.*, "Self‐Powered High‐Resolution and Pressure‐Sensitive Triboelectric Sensor Matrix for Real‐Time Tactile Mapping," *Advanced Materials,* vol. 28, no. 15, pp. 2896-2903, 2016.

[12] S. Yun, S. Park, B. Park *et al.*, "Polymer‐Waveguide‐Based Flexible Tactile Sensor Array for Dynamic Response," *Advanced Materials,* vol. 26, no. 26, pp. 4474-4480, 2014.

[13] B. C.-K. Tee, A. Chortos, A. Berndt *et al.*, "A skin-inspired organic digital mechanoreceptor," *Science,* vol. 350, no. 6258, pp. 313-316, 2015.

[14] S. Harada, K. Kanao, Y. Yamamoto *et al.*, "Fully printed flexible fingerprint-like three-axis tactile and slip force and temperature sensors for artificial skin," *ACS nano,* vol. 8, no. 12, pp. 12851-12857, 2014.

[15] R. S. Dahiya, P. Mittendorfer, M. Valle *et al.*, "Directions toward effective utilization of tactile skin: A review," *IEEE Sensors Journal,* vol. 13, no. 11, pp. 4121-4138, 2013.

[16] M. R. Cutkosky, R. D. Howe, and W. R. Provancher, "Force and tactile sensors," *Springer Handbook of Robotics*, pp. 455-476: Springer, 2008.

[17] Z. Kappassov, J.-A. Corrales, and V. Perdereau, "Tactile sensing in dexterous robot hands—Review," *Robotics and Autonomous Systems,* vol. 74, pp. 195-220, 2015.

[18] Y.-L. Park, B.-R. Chen, and R. J. Wood, "Design and fabrication of soft artificial skin using embedded microchannels and liquid conductors," *Sensors Journal, IEEE,* vol. 12, no. 8, pp. 2711-2718, 2012.

[19] L. Viry, A. Levi, M. Totaro *et al.*, "Flexible three‐axial force sensor for soft and highly sensitive artificial touch," *Advanced Materials,* vol. 26, no. 17, pp. 2659-2664, 2014.

[20] A. Hoffmann, A. Poeppel, A. Schierl *et al.*, "Environment-aware proximity detection with capacitive sensors for human-robot-interaction." pp. 145-150.

[21] H. Wang, G. de Boer, J. Kow *et al.*, "Design Methodology for Magnetic Field-Based Soft Tri-Axis Tactile Sensors," *Sensors,* vol. 16, no. 9, pp. 1356, 2016.

[22] G. d. Boer, N. Raske, H. Wang *et al.*, "Design Optimisation of a Magnetic Field Based Soft Tactile Sensor," *Sensors,* vol. 17, no. 11, pp. 2539, 2017.

[23] H. Wang, G. de Boer, J. Kow *et al.*, "A low-cost soft tactile sensing array using 3D Hall sensors," *Procedia Engineering,* vol. 168, pp. 650-653, 2016.

[24] A. J. Fleming, "A review of nanometer resolution position sensors: operation and performance," *Sensors and Actuators A: Physical,* vol. 190, pp. 106-126, 2013.

This article has been accepted for publication in a future issue of this journal, but has not been fully edited. Content may change prior to final publication. Citation information: DOI 10.1109/JSEN.2018.2845131, IEEE Sensors Journal

[25] A. Sophian, G. Tian, and M. Fan, "Pulsed eddy current non-destructive testing and evaluation: A review," *Chinese Journal of Mechanical Engineering,* vol. 30, no. 3, pp. 500, 2017.
[26] H. Wang, and Z. Feng, "Ultrastable and highly sensitive eddy current displacement sensor using self-temperature compensation," *Sensors and Actuators A: Physical,* vol. 203, pp. 362-368, 2013.
[27] H. Wang, Y. Liu, W. Li *et al.*, "Design of ultrastable and high resolution eddy-current displacement sensor system." pp. 2333-2339.
[28] H. Wang, J. Kow, N. Raske *et al.*, "Robust and high-performance soft inductive tactile sensors based on the Eddy-current effect," *Sensors and Actuators A,* vol. 271, pp. 44-52, 2018.
[29] Y. Wang, X. Yang, Y. Chen *et al.*, "A biorobotic adhesive disc for underwater hitchhiking inspired by the remora suckerfish," *Science Robotics,* vol. 2, no. 10, pp. eaan8072, 2017.
[30] H. Wang, J. W. Kow, N. Raske *et al.*, "Robust and High-Performance Soft Inductive Tactile Sensors based on the Eddy-Current Effect," *Sensors and Actuators A: Physical*, 2017.
[31] H. Wang, W. Li, and Z. Feng, "Noncontact thickness measurement of metal films using eddy-current sensors immune to distance variation," *IEEE Transactions on Instrumentation and Measurement,* vol. 64, no. 9, pp. 2557-2564, 2015.
[32] S. Ghosh, A. Mukherjee, K. Sahoo *et al.*, "A novel sensitivity enhancement technique employing wheatstone's bridge for strain and temperature measurement." pp. 1-6.
[33] "Inductance to digital converter LDC1614," June 25, 2017; http://www.ti.com/product/LDC1614/technicaldocuments.

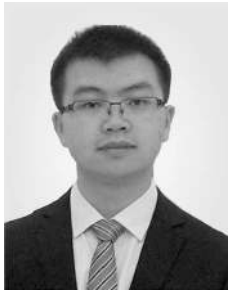

Hongbo Wang (M'14) is a Researcher at the Center for Micro-BioRobotics, Istituto Italiano di Tecnologia (IIT), Pontedera (Pisa), Italy. He recieved his B.E. and PhD in Precision Instrumentation and Machinery at the University of Science and Technology of China (USTC), Hefei, China, in 2010 and 2015 respectively. In 2015, he was awarded with the President's "*Special Prize*" of the Chinese Academy of Sciences for his PhD study. He is a grantee of the Marie Curie Fellowship (MSCA-IF-2017). His research interests include soft tactile and strain sensors, soft robotics, bioinspired design, self-powering sensors, sensing electronics, wearables, and smart materials.

Dominic Jones is a PhD student with School of Mechanical Engineering, University of Leeds, Leeds, UK, researching smart surgical tools for the prevention of damage. His research interests include smart surgical tools, soft tactile sensors, and haptic aids for surgical training.

Gregory de Boer is a Research & Teaching Fellow in the School of Mechanical Engineering, University of Leeds. His previous employment also includes a postdoctoral role at Imperial College London. His research interests are in numerical modelling, in particular computational fluid dynamics, non-linear solid mechanics, and optimisation. He has contributed toward publications in the fields of sensor design, lubrication flows, meta-modelling and external aerodynamics. He obtained his BEng, MEng and PhD degrees from the School of Mechanical Engineering, University of Leeds in 2011 and 2015 respectively.

Junwai Kow (S'18) received his B.Eng and M.Sc degree in mechatronics and robotics engineering from the University of Leeds, UK, in 2014 and 2015 respectively. Currently, he is pursuing his PhD in the research area of soft robotics at the University of Leeds. His research interests includes medical and rehabilitation robots.

Lucia Beccai (M'05) is a Tenure Track Senior Researcher at the Center for Micro-BioRobotics of the Istituto Italiano di Tecnologia (www.iit.it) of Pontedera, Italy, where she leads the group on Artificial Touch in Soft Biorobotics. Until 2009 she was Assistant Professor in Biomedical Engineering at Scuola Superiore Sant'Anna, Pisa, Italy. Her current research activities are on: smart tactile systems inspired from nature, soft robotic systems for investigating active and passive touch, milli- to micro-scale technologies for 3D soft sensing, and triboelectric-based powerless sensing. Target applications lie in soft robotics and wearable devices/human-computer interfaces. She has 3 patents and is author of more than 100 articles on refereed international journals, books, and international conference proceedings, is Associate Editor for journals of Scientific Reports and Frontiers in Robotics and AI, Soft Robotics Section.

Ali Alazmani (M'12) is a University Academic Fellow at the University of Leeds, United Kingdom. He completed his PhD in 2013 at the University of Leeds followed by a postdoctoral training at Harvard University, Wyss Institute of Biologically Inspired Engineering, and Boston Children's Hospital to develop a soft cardiac assist device. His research interests include design and fabrication of enabling technologies in soft systems, soft materials for sensing and actuation, and morphable soft-bodied robotics applied to healthcare and medical technologies.

Peter Culmer (M'15) is Associate Professor at the University of Leeds where he leads the multidisciplinary Surgical Technologies research group. Dr Culmer works closely with healthcare professionals and industry partners. His interests are the application of mechatronics to better understand, and address, worldwide healthcare challenges. His research achieves impact clinically and he plays an active part in the medical research community as board member of the NIHR MedTech in Surgical Technologies and iMechE's Biomedical Engineering Association. As academic lead of the EPSRC IMPRESS Network he is passionate about understanding and developing technology to help people with incontinence.